Chem. Res. Chinese Universities, 2020, 36(6), 1128—1135 doi: 10.1007/s40242-020-0320-y

Article

Fabrication of Fe-POMs as Visible-light-active Heterogeneous Photocatalyst

CEN Qing[1], XIAO Wei[1], LIU Yingqi[1], WANG Qi[1*],
NAFADY Ayman[3] and MA Shengqian[2*]

1. School of Environmental Science and Engineering, Zhejiang Gongshang University, Hangzhou 310018, P. R. China;

2. Department of Chemistry, University of North Texas, Denton, TX 76201, USA;

3. Department of Chemistry, College of Science, King Saud University, Riyadh 11451, Saudi Arabia

Abstract Visible-light-active Fe-POMs was fabricated *via* precipitating Fe^{3+} with Keggin type polyoxometalates ($H_3PW_{12}O_{40}$, $H_4SiW_{12}O_{40}$ or $H_3PMo_{12}O_{40}$) under solvothermal condition. The as-prepared Fe-POMs were denoted as FePW, FeSiW and FePMo, respectively. Among the three kinds of Fe-POMs, FePMo displayed the highest visible light absorption, the largest specific surface area, the most sensitive photocurrent response and the smallest charge transfer resistance, which were all beneficial for heterogeneous photocatalysis. The efficiency for Cr(VI) reduction was *ca*. 88% by FePMo after 50 min visible light irradiation. The estimated rate constant(0.042 min^{-1}) was *ca*. 2.5 and 1.8 times that by FePW and FeSiW, respectively. FTIR spectra indicated that the Keggin structure of $PMo_{12}O_{40}^{3-}$ was maintained in FePMo. Mechanism study indicated that the photogenerated electrons in LUMO and the holes in HOMO were thermodynamically feasible for Cr(VI) reduction and H_2O oxidation, respectively. Using FePMo as an optimized photocatalyst, good stability was also observed after 5 cyclic runs in both photocatalytic performance and XRD structure.

Keywords Cr(VI) reduction; Photocatalysis; Polyoxometalate; FePMo; Visible light

1 Introduction

Heavy metal chromium is widely used as a raw material in tanning, electroplating, printing, dyeing and other industries[1,2], resulting in a large amount of chromium-containing wastewater. If it is discharged into environment without proper treatment, human beings will suffer from huge health risks. Since the main oxidation states of chromium are Cr(VI) and Cr(III), the vital step for chromium remediation is the reduction of carcinogenic Cr(VI) to Cr(III), which can be easily precipitated and removed under alkaline conditions[3]. Compared with traditional methods[4,5], photocatalysis was considered as a green and energy-saving way[6]. Using the star photocatalyst(TiO_2) as an example, electron-hole pairs can be generated in the conduction band(CB) and valence band(VB) under UV light, respectively. Cr(VI) can be reduced to Cr(III) by capturing the photogenerated electrons in CB. However, due to the low proportion of ultraviolet light in solar radiation(<5%), the use of visible light (*ca*. 50%) has been widely concerned.

Different from metal oxide photocatalyst, polyoxometalates(POMs) are composed of metal oxygen clusters with more abundant composition and reversible redox properties[7—10]. Upon proper light irradiation, the electrons in POMs can jump from the highest occupied orbit(HOMO) to the lowest space orbit(LUMO), generating electron-hole pairs in excited $POMs^*$. Subsequently, reductive and oxidative reactions can be initiated. Using the most frequently studied Keggin type POMs ($H_3PW_{12}O_{40}$, $H_4SiW_{12}O_{40}$ or $H_3PMo_{12}O_{40}$) as example, they were successfully applied in the field of photolysis, including degradation of organic pollutants and reduction of heavy metal ions. Despite of this, they are soluble in water, leading to recovery difficulty. Thus, great efforts have been devoted to the development of heterogeneous POMs. Generally, immobilization on a substrate and precipitation with counter ions are two effective ways[11—14].

Typically, heterogeneous Keggin type POMs were fabricated *via* precipitation with monovalent counter ions(K^+, NH_4^+, Cs^+ or Ag^+). For example, $K_3PW_{12}O_{40}$ was obtained by precipitation of $H_3PW_{12}O_{40}$ with K^+ at room temperature followed by calcination at 450 ℃. Organic dyes(RhB, MG, MB and MV) can be photodegraded in the presence of H_2O_2. Visible-light-active $Cs_3PMo_{12}O_{40}$(CsPMo) was obtained by chemical etching of Cs_2CO_3 with $H_3PMo_{12}O_{40}$[15]. However, its efficiency for phenol degradation was limited. After 300 min visible light irradiation, it was less than 20% by pure CsPMo. $Ag_3PMo_{12}O_{40}$ was also fabricated *via* ball milling. Followed by *in-situ* photo-deposition, the $Ag/Ag_xH_{3-x}PMo_{12}O_{40}$ composite was obtained, which displayed boosted performance for either degradation of methyl

*Corresponding authors. Email: qiwang2021@163.com; Shengqian.Ma@unt.edu

Received October 7, 2020; accepted November 6, 2020.

Supported by the National Natural Science Foundation of China(No.21876154), the Natural Science Foundation of Zhejiang Province, China(No.LR18B070001), and partially supported by the Robert A. Welch Foundation(No.B-0027)(SM) and the Researchers Supporting Project(No.RSP-2020/79) at King Saud University(AN).

orange or reduction of Cr(VI)[16]. Recently, we also reported the fabrication of iron tungstosilicate(FeSiW) using Fe^{3+} as counter ion to precipitate with $H_4SiW_{12}O_{40}$ *via* solvothermal way. Cr(VI) can be rapidly photoreduced by FeSiW within 90 min[17].

In this study, the abundant and non-toxic Fe^{3+} was fixed as counter ion. $H_3PW_{12}O_{40}$, $H_4SiW_{12}O_{40}$ or $H_3PMo_{12}O_{40}$ was used as pristine POMs. Three kinds of visible-light-active Fe-POMs (FePW, FeSiW and FePMo) were fabricated under solvothermal conditions. The effects of different pristine POMs were systematically studied, including optical properties, specific surface area, photocurrent response and charge transfer resistance. In particular their photocatalytic performances were evaluated *via* reduction of Cr(VI) in aqueous media. The optimized Fe-POMs were further investigated in the field of operation conditions and cyclic experiments. Finally, the possible reaction mechanism was also proposed.

2 Experimental

2.1 Preparation of Fe-POMs

For the preparation of FePMo, equimolar(2 mmol) of $Fe(NO_3)_3·9H_2O$ and $H_3PMo_{12}O_{40}$ were mixed in 40 mL of methanol at room temperature. After stirring for 10 min, the mixture was transferred into a 100 mL Teflon-lined stainless-steel autoclave, followed by heating at 160 ℃ for 4 h. After cooling to room temperature, the precipitate was washed with ethanol and water, respectively. In the similar way, FePW and FeSiW were also prepared using $H_3PW_{12}O_{40}$ and $H_4SiW_{12}O_{40}$ in the initial step, respectively. The only difference is that the initial molar ratio of $Fe(NO_3)_3$ to $H_4SiW_{12}O_{40}$ was 4:3. The synthetic processes for different Fe-POMs are shown in Scheme 1.

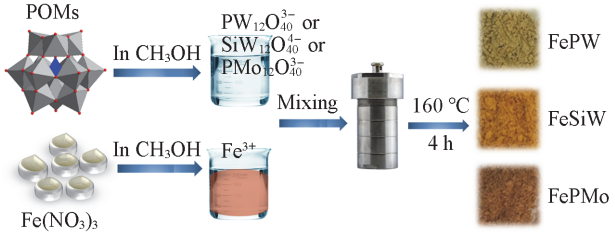

Scheme 1 Preparation processes for different Fe-POMs

2.2 Characterization

Three kinds of Fe-POMs(FePW, FeSiW and FePMo) powders were coated onto FTO as film electrodes. The photocurrent response, electrochemical impedance spectroscopy(EIS), and Mott-Schottky plots of the as-prepared films were monitored by an electrochemical workstation(CHI660E, Shanghai, China). The Brunauer-Emmett-Teller(BET) specific surface areas(S_{BET}) were measured by N_2 adsorption-desorption isotherms(Quantachrome Autosorb-IQ). UV-Vis diffuse reflectance spectra(UV-Vis DRS) were measured on a UV-visible spectrophotometer (Hitachi 3010). The optimized FePMo powder was characterized by X-ray diffraction(XRD, Rigaku D/Max 2500, Japan), Fourier transform infrared spectrometer(FTIR, Bruker VERTEX-70), and X-ray electron spectrometer(XPS, SCA lab 220i-XL). The generation of HO• radicals was monitored by electron spin resonance(ESR) spectroscopy(Bruker EPR ELEXSYS 500).

2.3 Photoelectrochemical Analysis

The photoelectrochemical properties were tested on a CHI 660E electrochemical workstation(Shanghai Chenhua Instrument Co., Ltd., China), and the three-electrode system was used in the test. The specific operation was as follows: at room temperature, a xenon lamp(XQ 500 W, Shanghai Lansheng Electronics Co., Ltd., China) was used as the light source. A filter was applied to ensure visible light($\lambda \geqslant 420$ nm) with 100 mW/cm^2 intensity. The platinum plate and Ag/AgCl electrode were used as counter electrode and reference electrode, respectively. Photocurrent response was monitored through time-current curves(*i-t* curves, applied voltage: 0.2 V *vs.* Ag/AgCl,) in 0.1 mol/L Na_2SO_3-Na_2SO_4 mixed solution. The EIS Nyquist plots were tested in 0.5 mol/L Na_2SO_4 solution with no external voltage during the measurements. Mott-Schottky plots were tested in 0.5 mol/L Na_2SO_4 solution in the shielding box.

2.4 Photocatalytic Experiment

The photocatalytic performances of the as-prepared Fe-POMs were evaluated using Cr(VI) as target pollutant. The light source was a 300 W Xe lamp(CEL-300, Beijing Zhongjiao Jinyuan Co., Ltd., China) equipped with a filter to ensure visible light($\lambda \geqslant 420$ nm). Photocatalyst(50 mg) was added to a beaker containing 50 mL of Cr(VI) aqueous solution (80 μmol/L) in the presence of 2 mmol/L EDTA-2Na. Before photocatalysis, the suspension was stirred in the dark for 30 min to ensure adsorption-desorption equilibrium. Upon visible light irradiation, the suspension was sampled every 10 min and separated by centrifugation. The concentration of Cr(VI) in the supernatant was determined by 1,5-diphenyl carbazide colorimetric method[17], using characteristic maximum absorption(544 nm) as monitoring wavelength.

3 Results and Discussion

3.1 Optical Response

In this study, three types of Fe-POMs(FePW, FeSiW and FePMo) were prepared *via* solvothermal method. Their optical properties were compared *via* measuring UV-Vis-DRs spectra and digital photos. As shown in Fig.1(A) and Scheme 1, the deep yellow FePMo powder displayed the highest absorption in visible light region. The corresponding band gap(E_g) was estimated to be 2.53 eV[Fig.1(B)], which was narrower than that of FePW(2.83 eV) and FeSiW(2.70 eV).

Although in most cases, narrower band gap is beneficial for photocatalysis under visible light, there is no absolute correlation between E_g and photocatalytic performance. The photoexcitation is only the first step of photocatalysis, and the separation of electron-hole pairs has a significant impact on the photocatalytic performance. Thus, photoelectrochemical measurements were further carried out to study the excitation,

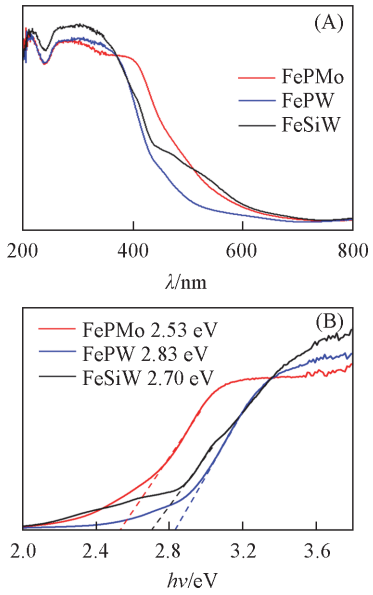

Fig.1 UV-Vis-DRS spectra(A) and corresponding Tauc plots(B) of FePMo, FePW and FeSiW

separation and transfer of photo-generated charge carriers.

3.2 Photoelectrochemical Properties

As shown in Fig.2(A), FePMo exhibited the highest photocurrent density, indicating the most sensitive photocurrent response. Besides, EIS Nyquist plots were used to analyze the interfacial transfer behavior of photogenerated charges. As shown in Fig.2(B), the radius of arc reflects the charge transfer resistance. The smaller the radius of the circular arc, the faster the charge transfer rate[18]. Thus, it can be deduced that FePMo has the lowest charge transfer resistance. Considering the above optical and photoelectrochemical properties, FePMo can be considered as a highly active candidate for photocatalytic applications.

3.3 BET and SEM Analysis

For a heterogeneous photocatalyst, the BET specific surface area(S_{BET}) was another important factor, which may influence the photocatalytic performance. Typically, larger S_{BET} indicates more surface active sites, which may be beneficial for photocatalysis. Herein, the N_2 adsorption-desorption isotherms of the as-prepared Fe-POMs were further measured to estimate the S_{BET}. The results are displayed in Fig.3. It can be observed that the calculated values of S_{BET} for the three systems followed the order of FePMo(40.8 m^2/g)>FeSiW(8.0 m^2/g)>FePW

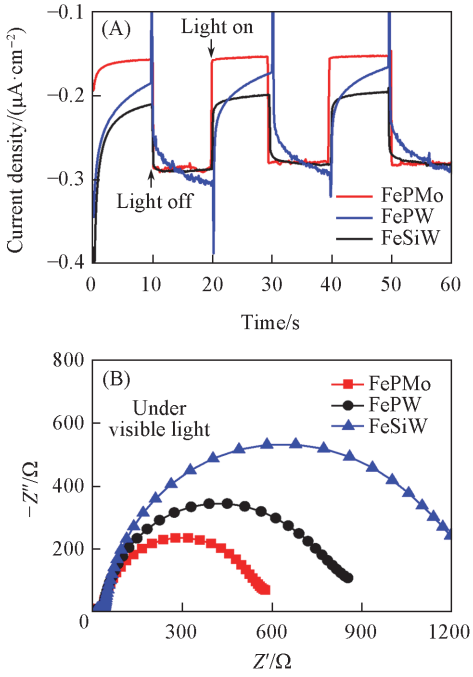

Fig.2 Photocurrent response(A) and EIS Nyquist plots(B) of FePMo, FePW and FeSiW

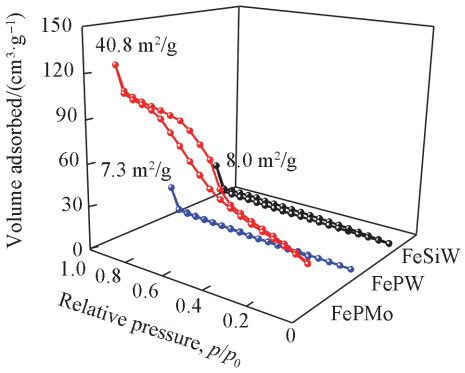

Fig.3 Comparison of BET surface areas of different Fe-POMs

(7.3 m^2/g). Since FePMo displayed the highest S_{BET}, it was selected as the optimized sample for following structural analysis.

To further investigate the surface structure, the morphology of FePMo was investigated by SEM and the results are illustrated in Fig.4. It can be observed that the diameters of FePMo spheres mostly ranged from 3 μm to 5 μm[Fig.4(A)]. Besides, the enlarged picture of the broken sphere indicated that it is composed of many small particles[Fig.4(C)], which may be the reason for the large specific surface area.

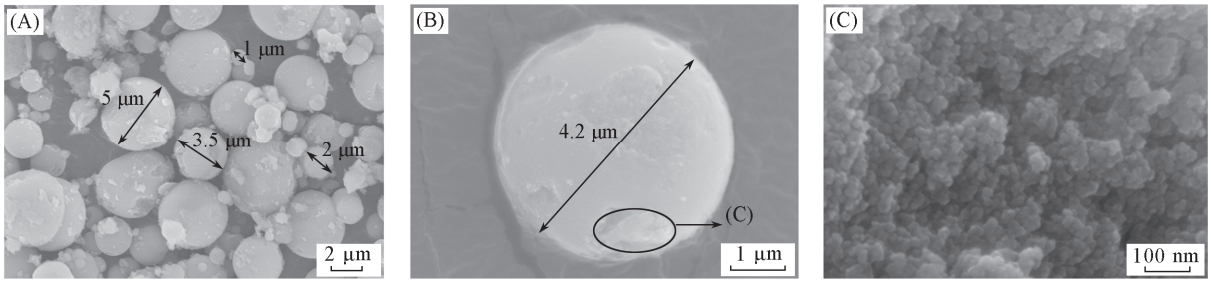

Fig.4 SEM images of FePMo under different scales

3.4 Structural Analysis

In order to probe possible structural changes of $H_3PMo_{12}O_{40}$ induced by precipitation with Fe^{3+}, the XRD patterns were compared and the results are shown in Fig.5(A). It is obvious that $H_3PMo_{12}O_{40}$ displayed distinct XRD peaks at 2θ=7.2°, 20.5° and 27.2°. Comparing with characteristic peaks in JCPDS No.09-0412, Keggin structure of phosphomolybdate phase can be confirmed[19]. As for FePMo, the broad region at 2θ=20°—40° indicated its amorphous state[20]. Such difference may be ascribed to the changes of secondary structure in POMs, such as the three-dimensional arrangement[21].

For more structural information, FTIR spectra were further carried out to determine the vibrational peaks associated with chemical bonds[Fig.5(B)]. It can be observed that the Keggin structure of $PMo_{12}O_{40}^{3-}$ was maintained in FePMo. In the pristine $H_3PMo_{12}O_{40}$, the characteristic peaks corresponding to ν(P—O), ν(Mo—O) and ν(Mo—O—Mo) appeared at 1063, 960, 868 and 776 cm^{-1}, respectively. As for FePMo, the characteristic P—O, Mo—O and Mo—O—Mo vibrations can still be observed, but with slight shift[22].

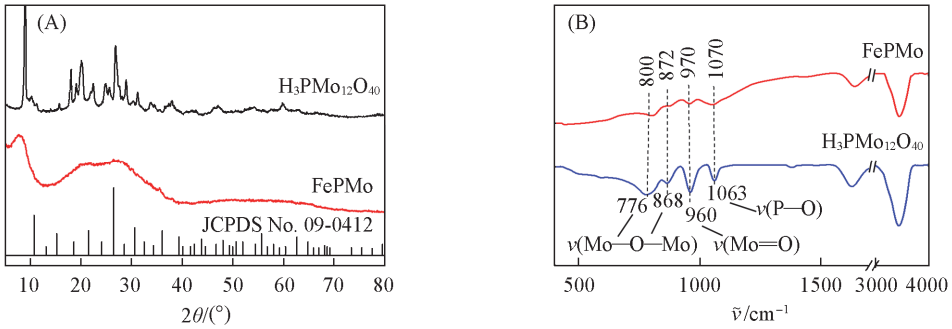

Fig.5 XRD patterns(A) and FTIR spectra(B) of FePMo and $H_3PMo_{12}O_{40}$

The FePMo sample was further characterized by XPS technique to obtain the information of surface element compositions and chemical states. The XPS survey spectrum was illustrated in Fig.6(A). Obvious signals corresponding to Fe, O, P and Mo elements can be detected. High resolution spectra of Mo_{3d}, Fe_{2p} and P_{2p} were also deconvoluted. For example, as for Mo_{3d} [Fig.6(B)], the binding energy peaks centered at 235.8 ($Mo_{3d_{3/2}}$) and 232.5 eV($Mo_{3d_{5/2}}$) were attributed to Mo^{6+} in Mo—O bond[23]. As for Fe_{2p}[Fig.6(C)], the peaks at 712.6($Fe_{2p_{3/2}}$) and 725.8 eV($Fe_{2p_{1/2}}$) were attributed to Fe^{3+}. Consistent with previous reports[24], the $Fe_{2p_{3/2}}$ can be devolved into multiple peaks. Meanwhile, there were no Fe^{2+} shakeup satellite peaks(*ca.* 715 eV). As for P_{2p}[Fig.6(D)], the peak at 133.8 eV was ascribed to surface PO_4^{3-} species[25]. Thus, it can be deduced that the chemical states of Fe, P and Mo in FePMo were well maintained, which were the same as those in the original $H_3PMo_{12}O_{40}$.

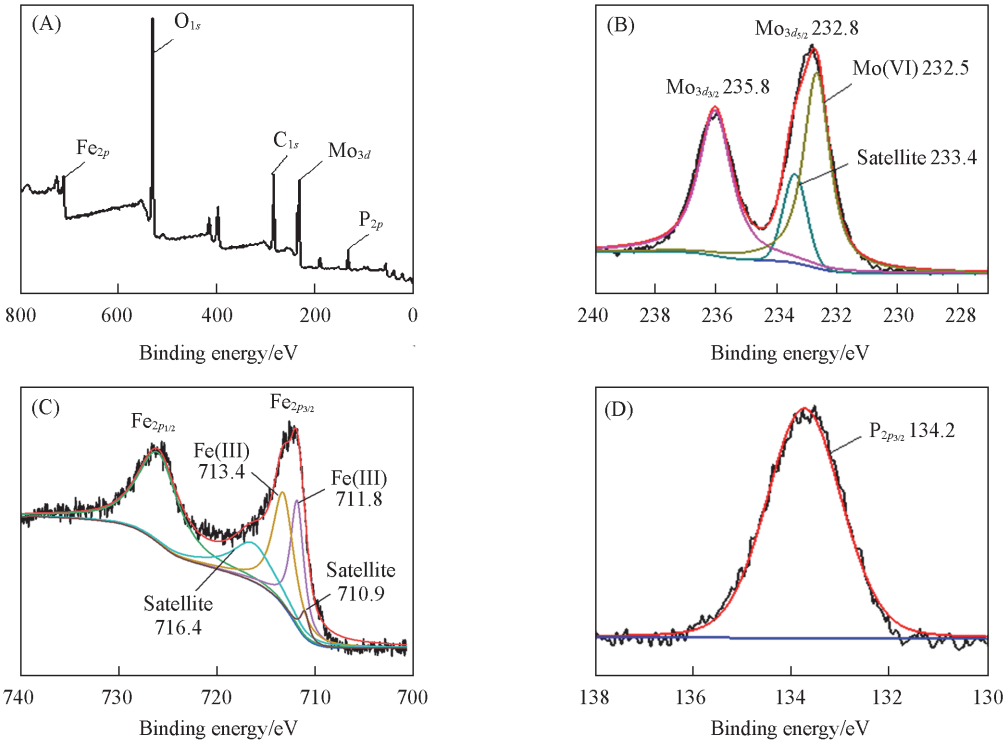

Fig.6 Survey XPS spectra(A) and high resolution XPS spectra of Mo_{3d}(B), Fe_{2p}(C) and P_{2p}(D) of FePMo

3.5 Photocatalytic Activity

The photocatalytic performances of the as-prepared Fe-POMs were evaluated *via* Cr(VI) reduction. As shown in Fig.7(A), among the three tested samples, FePMo displayed the highest photocatalytic performance. Under visible light irradiation, the reduction efficiency for Cr(VI) reached 88% within 50 min. Whereas, the values were 58% and 69% by FePW and FeSiW, respectively. Control experiments in the dark were also performed using FePMo as catalyst. It is obvious that the reduction of Cr(VI) was negligible. Besides, the initial adsorption amounts of Cr(VI) on different Fe-POMs were also compared and the results are listed in Table S1(see the Electronic Supplementary Material of this paper). After 30 min dark reaction, the adsorption amount was 5.1% on FePMo, which was much less than that on FeSiW or FePW.

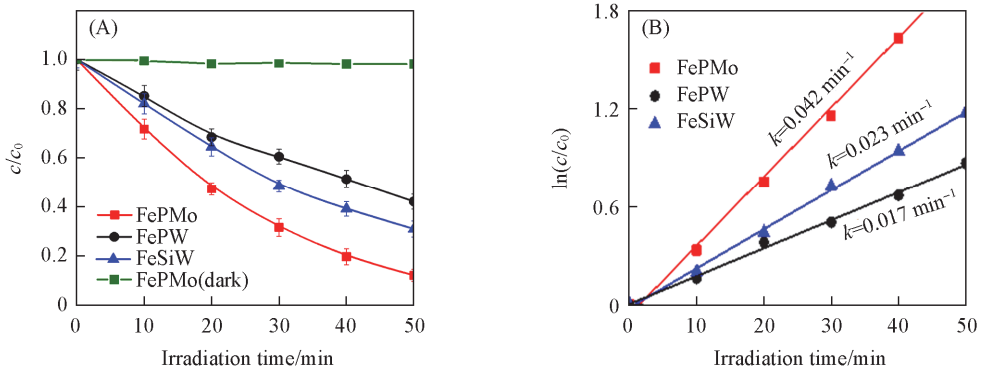

Fig.7 Photocatalytic reduction of Cr(VI) at pH=2 with 1.0 g/L different Fe-POMs(A) and corresponding pseudo-first-order kinetic curves(B)

To further confirm the importance of FePMo, more supplementary experiments were performed. First, if $H_3PMo_{12}O_{40}$ was not added, only 2 mmol of $Fe(NO_3)_3{\cdot}9H_2O$ was dissolved in methanol for solvent thermal reaction, and red precipitate was produced. Second, if $Fe(NO_3)_3{\cdot}9H_2O$ was not added, only $H_3PMo_{12}O_{40}$ was treated in the same way, no precipitate was found. As shown in Fig.S1(see the Electronic Supplementary Material of this paper), the reduction of Cr(VI) was negligible after 50 min visible light irradiation by pure $H_3PMo_{12}O_{40}$. The reduction efficiency was *ca*. 50% by the red precipitate, which is far lower than that by FePMo. In addition, partial dissolution of the red precipitate can be directly observed. The value of Fe^{3+} leaching in the red precipitate suspension was calculated to be 204.2 mg/L. However, less than 0.1 mg/L Fe^{3+} was detected in the suspension of FePMo (Fig.S2, see the Electronic Supplementary Material of this paper), which further confirm the superiority of FePMo.

The estimated pseudo-first-order rate constant was 0.042 min^{-1} by FePMo[Fig.7(B)], which was *ca*. 2.5 and 1.8 times that by FePW and FeSiW, respectively. Additionally, it should be noted that FePW was not stable and easily dissolved under the present condition. Therefore, FePMo was selected as the optimal Fe-POMs in the following studies.

For the photocatalytic reduction of Cr(VI), the effect of operating factors(initial solution pH, concentration of coexisting organics, catalyst loading amount) were further investigated. As shown in Fig.8(A), the reduction of Cr(VI) was accelerated at acidic pH. Higher pH was deleterious to the reduction of Cr(VI). In particular, the activity dramatically decreased to *ca*. 10% at pH 8. This can be attributed to the larger thermodynamic driving force and consumption of H^+ during the reduction of Cr(VI)[26—28]. With the decrease of pH, the thermodynamic driving potential exhibited 78 mV/pH enhancement, due to the difference between E_{CB}(59 mV/pH) and $E_{Cr(VI)/Cr(III)}$(138 mV/pH). Furthermore, at different solution pH values, Cr(VI) may exist in different forms, such as $Cr_2O_7^{2-}$ and CrO_4^{2-} in alkaline media, $Cr_2O_7^{2-}$ and $HCrO_4^-$ under acidic conditions. For all the forms of Cr(VI), H^+ was always consumed during the reduction of Cr(VI) according to equations.

$$14H^+ + Cr_2O_7^{2-} + 6e^- \longrightarrow 2Cr^{3+} + 7H_2O \quad (1)$$

$$8H^+ + CrO_4^{2-} + 3e^- \longrightarrow Cr^{3+} + 4H_2O \quad (2)$$

$$7H^+ + HCrO_4^- + 3e^- \longrightarrow Cr^{3+} + 4H_2O \quad (3)$$

$$6H^+ + H_2CrO_4 + 3e^- \longrightarrow Cr^{3+} + 4H_2O \quad (4)$$

In addition, the effect of coexisting organics(EDTA-2Na) was also studied. The results in Fig.8(B) indicated that the presence of organics can promote the reduction of Cr(VI). When the concentration of EDTA-2Na increased from 0.5 mmol/L to 2 mmol/L, the reduction efficiency increased from *ca*. 20% to 88% after 50 min visible light irradiation. When the concentration was further increased to 3 mmol/L, Cr(VI) can be nearly 100% reduced within 20 min. Herein, the presence of organics may act as a hole scavenger[28,29], which may promote the separation of photogenerated electron-hole pairs.

The effect of FePMo loading amount was also investigated. As shown in Fig.8(C), the reduction of Cr(VI) was accelerated with increasing the FePMo amount. The growth trend slows down when the loading amount was larger than 1.0 g/L. Considering both economic and practical aspects, 1.0 g/L was selected as the optimal one. Additionally, the effect of initial Cr(VI) concentration was also studied. As shown in Fig.S3(see the Electronic Supplementary Material of this paper), higher concentration of Cr(VI) was further studied. After 150 min visible light irradiation, 160 μmol/L Cr(VI) can be completely reduced by FePMo. Such performance was good comparing with similar POMs as well as star TiO_2(Table S2, see the Electronic Supplementary Material of this paper). Pure POMs($H_3PW_{12}O_{40}$ and $H_3PMo_{12}O_{40}$) and TiO_2 displayed weaker photocatalytic

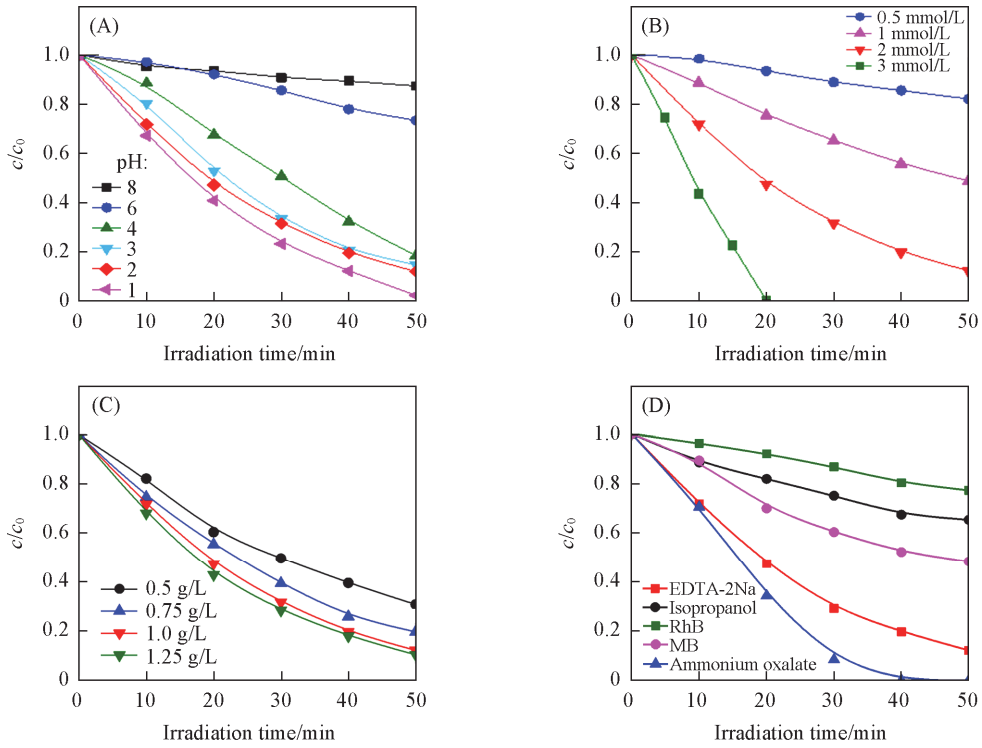

Fig.8 Effect of initial solution pH(A), coexisting EDTA-2Na concentration(B), catalyst loading amount(C) and coexisting organic types(D) on the reduction of Cr(VI) by FePMo under visible light

performance relative to FePMo, and some of them only worked under UV light. Higher activity can be observed when noble metals(such as Ag and Pt) were loaded. In general, considering both application cost and efficiency, the as-prepared FePMo has some advantages.

Finally, the effect of coexisting organic types was studied. As shown in Fig.8(D), with a fixed concentration(2 mmol/L organics), the reduction of Cr(VI) was different. The results indicated that EDTA-2Na and ammonium oxalate had more stronger accelerating effect than others.

3.6 Stability of FePMo

For a good photocatalyst, high performance and good stability are two important metrics in practical applications. Herein, the stability of FePMo was firstly investigated after 5 successive runs, and the results are displayed in Fig.9. The reaction conditions were: initial pH 2, 1.0 g/L FePMo and 2.0 mmol/L EDTA-2Na. After 5 cycles, the photocatalytic performance was well maintained[Fig.9(A)]. Importantly, possible changes in structure were investigated by XRD analysis. As shown in Fig.9(B), similar XRD patterns of FePMo can also be observed before and after cyclic experiments, indicating the stability of crystal structure. Furthermore, the leaching of Fe^{3+} in the dark and during the photocatalytic reaction process was monitored using 10-phenanthroline colorimetric method. The concentration of leached Fe^{3+} was calculated from the stand curves. As shown in Fig.S2, after 50 min under visible light, the concentration of dissolved Fe^{3+} was less than 0.15 mg/L. Assuming that the initial added FePMo powder(50 mg) was totally dissolved in 50 mL of reaction solution, the maximum concentration of dissolved Fe^{3+} was *ca*. 29.5 mg/L. Thus, the percentage of Fe^{3+} leaching after each cycle was less than 1% at pH 2. At a higher pH value, such as pH 8, the leaching was slightly higher(Fig.S4, see the Electronic Supplementary Material of this paper). After 50 min visible light irradiation, the leaching of Fe^{3+} was less than 0.3 mg/L.

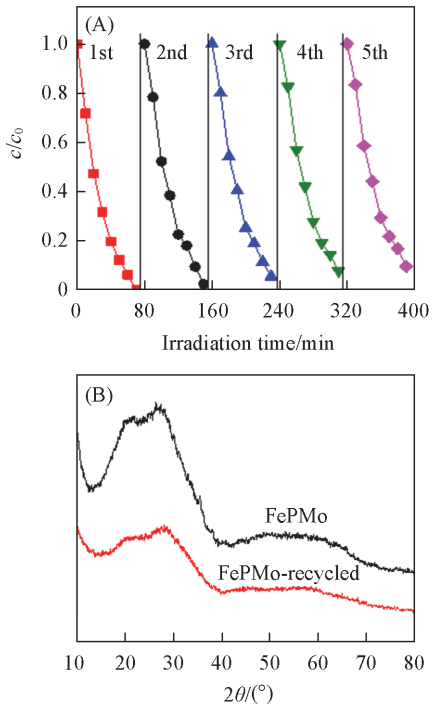

Fig.9 Photocatalytic reduction of Cr(VI) by FePMo in 5 consecutive cyclic runs(A) and comparison of XRD patterns between fresh and recycled FePMo(B)

3.7 Proposed Mechanism

In this work, visible-light-active FePMo displayed high photocatalytic performance for Cr(VI) reduction, which can be ascribed to efficient generation and separation of photogenerated charges. In order to understand this, we need to know the positions of LUMO and HOMO in FePMo. As a POMs salt, the LUMO and HOMO position of FePMo was similar to the conduction band(CB) and valence band(VB) in a semiconductor, respectively. The positive slope of Mott-Schottky plots indicates the n-type nature of the catalyst. Besides, the CB position(E_{CB}) of an n-type photocatalyst is *ca*. 0.1 V more negative than the flat band. The flat band potential(E_{fb}) can be obtained from Mott-Schottky plots. Thus, E_{CB} can be calculated according to Eq.(5):

$$E_{CB} = E_{fb} - 0.1 \quad (5)$$

Moreover, the band gap(E_g) was the difference between the maximum energy of VB and the minimum energy of CB, which can be obtained by UV-Vis DRS spectrum, and calculated using Eq.(6):

$$E_g = E_{VB} - E_{CB} \quad (6)$$

Thus, in this way, the position of VB can be calculated[30]. As shown in Fig.10(A), positive slope in Mott-Schottky plots indicated n-type behavior of FePMo. Besides, E_{fb} was estimated to be –0.3 V *vs.* Ag/AgCl(or –0.1 V *vs.* NHE). Thus, the LUMO position(E_{CB}) can be deduced to be –0.2 V *vs.* NHE. Moreover, the corresponding E_g of FePMo was *ca*. 2.53 eV by UV-Vis-DRS spectra[Fig.1(B)]. Thus, the HOMO position can be calculated to be 2.33 V *vs.* NHE.

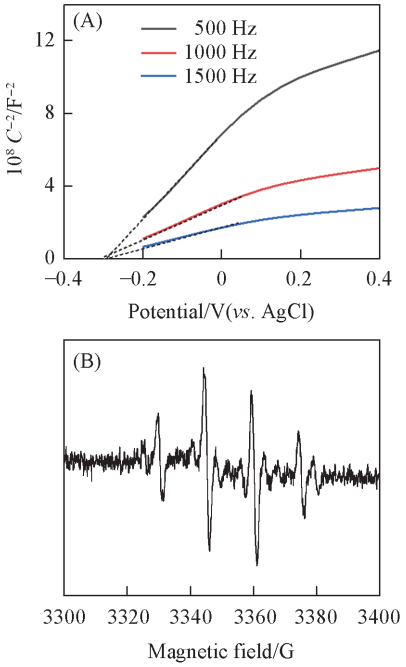

Fig.10 Mott-Schottky plots of FePMo at different frequencies(A) and typical DMPO-HO• signals monitored by ESR(B)

Since the LUMO position(–0.2 V) is more negative than $E_{Cr(VI)/Cr(III)}$(0.51 V)[31,32], the electron transfer from the LUMO of FePMo to Cr(VI) is thermodynamically feasible. Meanwhile, the HOMO position(2.33 V) is energetic enough for the oxidation of surface hydroxyl groups($E_{OH^-/•OH}$=1.99 V)[33]. Thus, the generation of highly oxidative HO• radicals was thermodynamically feasible. Indeed, the formation of HO• was further confirmed by ESR experiment. As shown in Fig.9(B), distinct DMPO-HO• signals can detected. Therefore, according to the above analysis, a proposed mechanism for Cr(VI) reduction by FePMo is depicted in Fig.11. Under visible light irradiation, photogenerated electrons in the LUMO of FePMo can be transferred to Cr(VI), leading to the reduction of Cr(VI). The holes in HOMO can directly oxidize organics or induce the generation of active HO• radicals.

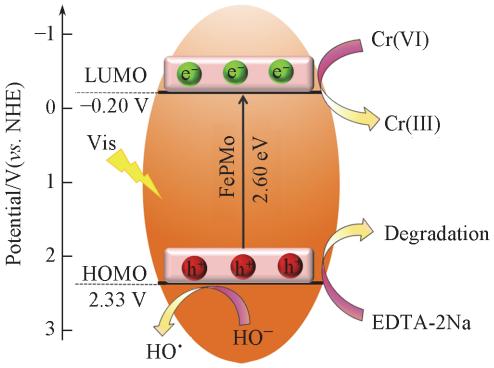

Fig.11 Proposed charge transfer mechanism over FePMo under visible light irradiation

4 Conclusions

In summary, we reported the fabrication of three kinds of visible-light-active Fe-POMs(FePW, FeSiW and FePMo) photocatalysts using solvothermal procedure. Among which, FePMo displayed highest photocatalytic activity for Cr(VI) reduction. The reason can be attributed to the suitable visible-light response and photoelectrochemical properties, which were beneficial for the generation, separation and transfer of electron-hole pairs. Moreover, the FePMo powder has good stability in cyclic runs even under acidic condition. This present study provides the access to a series of efficient and highly stable candidates for heterogeneous POMs photocatalysis in environmental remediation.

Electronic Supplementary Material

Supplementary material is available in the online version of this article at http://dx.doi.org/10.1007/s40242-020-0320-y.

References

[1] Carlos E. B., Violeta L., Bryan B., *J. Hazard. Mater.*, **2012**, *223/224*, 1

[2] Wang C., Du X., Li J., Guo X., Wang P., Zhang J., *Appl. Catal. B: Environ.*, **2016**, *193*, 198

[3] Zou Y., Wang X., Khan A., Wang P., Liu Y., Alsaedi A., Hayat T., Wang X., *Environ. Sci. Technol.*, **2016**, *50*, 7290

[4] Al-Shannag M., Al-Qodah Z., Bani-Melhem K., Qtaishat M. R., Alkasrawi M., *Chem. Eng. J.*, **2015**, *260*, 749

[5] Fu F., Wang Q., *J. Environ. Manage.*, **2011**, *92*, 407

[6] Chen C., Ma W., Zhao J., *Chem. Soc. Rev.*, **2010**, *39*, 4206

[7] An X., Tang Q., Lan H., Liu H., Qu J., *Appl. Catal. B: Environ.*, **2019**,

244, 407

[8] Zhang G., Yang W., Wu W., Wu X., Zhang L., Kuang X., Wang S., Lu C., *J. Catal.*, **2019**, *369*, 54

[9] Zhao X., Zhang Y., Zhao Y., Tan H., Zhao Z., Shi H., Wang E., Li Y., *Dalton Trans.*, **2019**, *48*, 6484

[10] Tang Q., An X., Lan H., Liu H., Qu J., *Appl. Catal. B: Environ.*, **2020**, *268*, 118394

[11] Huang Y., Wang R., *J. Mater. Chem. A*, **2019**, *7*, 12105

[12] Liu W., Dong L., Li R., Chen Y., Sun S., Li S., Lan Y., *ACS Appl. Mater. Interf.*, **2019**, *11*, 7030

[13] Tangestaninejad S., Mirkhani V., Moghadam M., Mohammadpoor-Baltork I., Shams E., Salavati H., *Ultrason. Sonochem.*, **2008**, *15*, 438

[14] Koutsouroubi E. D., Xylouri A. K., Armatas G. S., *Chem. Commun.*, **2015**, *51*, 4481

[15] Wang Q., Liu E., Zhang C., Huang S., Cong Y., Zhang Y., *J. Colloid. Interf. Sci.*, **2018**, *516*, 304

[16] Shi H., Yan G., Zhang Y., Tan H., Zhou W., Ma Y., Li Y., Chen W., Wang E., *ACS Appl. Mater. Interfaces*, **2017**, *9*, 422

[17] Cen Q., Gao Q., Zhang C., Liu Y., Wang Q., Wang Q., *J. Colloid Interf. Sci.*, **2020**, *562*, 12

[18] Gao Q., Lin D., Fan Y., He Q., Wang Q., *Chem. Eng. J.*, **2019**, *374*, 10

[19] Fournier M., Feumi-Jantou C., Rabia C., Hervé G., Launay S., *J. Mater. Chem.*, **1992**, *2*, 971

[20] Al-Garni T., Al-Jallal N., Aouissi A., *J. Chem.*, **2017**, *2017*, 5641604

[21] Yin D., Zhang L., Zhao X., Chen H., Zhai Q., *Chin. J. Catal.*, **2015**, *36*, 2203

[22] Silva M. J., Liberto N. A., De Andrade L. L. C., Pereira U. A., *J. Mol. Catal A: Chem.*, **2016**, *422*, 69

[23] Spojakina A., Kraleva E., Jiratova K., Petrov L., *Appl. Catal. A: Gen.*, **2005**, *288*, 10

[24] Grosvenor A. P., Kobe B. A., Biesinger M. C., McIntyre N. S., *Surf. Interface Anal.*, **2004**, *36*, 1564

[25] Phillips D. C., Sawhill S. J., Self R., Bussell M. E., *J. Catal.*, **2002**, *207*, 266

[26] Wang Q., Shi X., Xu J., Crittenden J. C., Liu E., Zhang Y., Cong Y., *J. Hazard. Mater.*, **2016**, *307*, 213

[27] Cong Y., Ji Y., Ge Y., Jin H., Zhang Y., Wang Q., *Chem. Eng. J.*, **2017**, *307*, 72

[28] Wang Q., Zhu N., Liu E., Fu L., Zhou T., Cong Y., *Electrochim. Acta*, **2016**, *216*, 266

[29] Tian H., Araya T., Li R., Fang Y., Huang Y., *Appl. Catal. B*: *Environ.*, **2019**, *254,* 371

[30] Dong G., Zhang Y., Pan Q., Qiu J., *J. Photoch. Photobio. C*, **2014**, *20*, 33

[31] Wu Q., Zhao J., Qin G., Wang C., Tong X., Song X., *Appl. Catal. B: Environ.*, **2013**, *142*, 142

[32] Zhao Z., Zhang W., Sun Y., Yu J., Zhang Y., Wang H., Dong F., Wu Z., *J. Phys. Chem. C*, **2016**, *120*, 11889

[33] Liu B., Liu X., Liu J., Feng C., Li Z., Li C., Gong Y., Pan L., Xu S., Sun C. Q., *Appl. Catal. B: Environ.*, **2018**, *226*, 234